Rapid hippocampal plasticity supports motor sequence learning

Florencia Jacobacci[a], Jorge L. Armony[b], Abraham Yeffal[a], Gonzalo Lerner[a], Edson Amaro Jr[c], Jorge Jovicich[d], Julien Doyon[e,f], and Valeria Della-Maggiore[a,1]

[a]Instituto de Fisiología y Biofísica (IFIBIO) Houssay, Consejo Nacional de Investigaciones Científicas y Técnicas (CONICET), Departamento de Fisiología y Biofísica, Universidad de Buenos Aires, Buenos Aires, 1121, Argentina; [b]Douglas Mental Health Research Institute, McGill University, Montreal, QC, H4H 1R3, Canada; [c]Plataforma de Imagens na Sala de Autopsia (PISA), Instituto de Radiologia, Facultade de Medicina, Universidade de Sao Paulo, Sao Paulo, 05403-000, Brazil; [d]Center for Mind/Brain Sciences, University of Trento, Rovereto, 38068, Trento, Italy; [e]McConnell Brain Imaging Center, Montreal Neurological Institute, McGill University, Montreal, QC, H3A 2B4, Canada; and [f]Department of Neurology and Neurosurgery, McGill University, Montreal, QC, H3A 2B4, Canada

Edited by David J. Heeger, New York University, New York, NY, and approved July 28, 2020 (received for review May 20, 2020)

Recent evidence suggests that gains in performance observed while humans learn a novel motor sequence occur during the quiet rest periods interleaved with practice (micro-offline gains, MOGs). This phenomenon is reminiscent of memory replay observed in the hippocampus during spatial learning in rodents. Whether the hippocampus is also involved in the production of MOGs remains currently unknown. Using a multimodal approach in humans, here we show that activity in the hippocampus and the precuneus increases during the quiet rest periods and predicts the level of MOGs before asymptotic performance is achieved. These functional changes were followed by rapid alterations in brain microstructure in the order of minutes, suggesting that the same network that reactivates during the quiet periods of training undergoes structural plasticity. Our work points to the involvement of the hippocampal system in the reactivation of procedural memories.

hippocampus | structural plasticity | functional MRI | reactivation | motor sequence learning

Information transfer from the hippocampus to long-term storage sites in the neocortex plays a key role in the consolidation of declarative and spatial memories. A proposed mechanism mediating consolidation is the replay of behavioral sequences in the hippocampus during sharp-wave ripples (1). In the last decade, there has been substantial work suggesting that, in humans, hippocampal reactivation after learning relates to memory consolidation (2–4). Recently, Bönstrup et al. (5) described a pattern of gains in performance during the quiet—rest—periods of motor sequence learning (MSL) that is reminiscent of the behavioral benefits produced by task replay in rodents (6). These rapid improvements in performance, known as micro-offline gains (MOGs) (5), differ from long-term offline gains induced by sleep-dependent hippocampal consolidation (7), in that they are short-term. Whether the hippocampus is also involved in the production of MOGs remains currently unknown.

Here, we explored how these short-term and long-term aspects of motor skill memory impact on brain microstructure (Fig. 1*A*). To this end, we first used functional magnetic resonance imaging (fMRI) during MSL to identify the brain areas associated with MOGs. Additionally, we assessed the time course of microstructural changes in mean diffusivity (MD), a diffusion-weighted imaging (DWI) proxy of structural plasticity in humans (8–10). An active motor task involving no learning served as control (CTL) for nonspecific microstructural changes induced by motor practice. To differentiate between short-term and long-term plasticity, DWIs were acquired before and 30 min and 24 h after task performance.

Results and Discussion

Subjects learned a novel five-item motor sequence in a self-paced manner (Fig. 1*B*) (7). We found that MOGs, which explained most of the variance during learning (Fig. 1 *B*, *Inset* and *C*), were greatest during the first half of training (linear mixed model with learning stage [early, late] as fixed effect, $P = 0.0094$), i.e., before reaching asymptotic performance (Fig. 1*D*). Whole-brain analysis of the fMRI data showed that cortico-cerebellar and cortico-striatal systems were most active during task execution (Fig. 2*A*), a finding that is in agreement with previous studies (11). In contrast, the hippocampus and the precuneus, which were functionally connected across Rest and Task blocks ($r = 0.73$, $P < 0.0001$; repeated-measures correlation), showed greater activity during the periods of quiet rest than during task execution (Fig. 2*A*). Like MOGs, increments in blood-oxygen-level-dependent (BOLD) during rest were strongest in the first half of training (linear mixed model with learning stage (early, late), as fixed effect—Bonferroni corrected—hippocampus $P = 0.047$; precuneus $P = 0.006$). Critically, the BOLD signal in these structures predicted the magnitude of MOGs, but only during the early stages of learning, i.e., before reaching the asymptote (hippocampus early: $r = 0.51$, $P = 0.035$, late: $r = 0.081$, $P = 0.76$; precuneus, early: $r = 0.6$, $P = 0.012$, late: $r = 0.25$, $P = 0.33$). Importantly, and in agreement with Bönstrup et al. (5), MOGs did not correlate with overnight offline gains in performance ($r = 0.079$, $P = 0.75$). These results may reflect a

Significance

Learning predefined sequences of actions is of everyday importance. Recent evidence suggests that improvements in performance associated with learning a motor sequence take place during the quiet rest periods interleaved with practice. This phenomenon known as micro-offline gains (MOGs) is different from offline gains in performance observed overnight. Using a multimodal—functional and structural—MRI approach, here we show that the hippocampus participates in the generation of MOGs through a mechanism reminiscent of memory reactivation. Our findings point to the involvement of the hippocampus in the reactivation of nonhippocampal memories and provide evidence for a possible common mechanism at the basis of the formation of declarative and nondeclarative memories.

Author contributions: J.D. and V.D.-M. designed research; F.J., A.Y., and G.L. performed research; F.J., J.L.A., E.A., and J.J. contributed new reagents/analytic tools; F.J., J.L.A., A.Y., and V.D.-M. analyzed data; and F.J. and V.D.-M. wrote the paper.

The authors declare no competing interest.

This article is a PNAS Direct Submission.

[1]To whom correspondence may be addressed. Email: vdellamaggiore@fmed.uba.ar.

This article contains supporting information online at https://www.pnas.org/lookup/suppl/doi:10.1073/pnas.2009576117/-/DCSupplemental.

First published September 8, 2020.

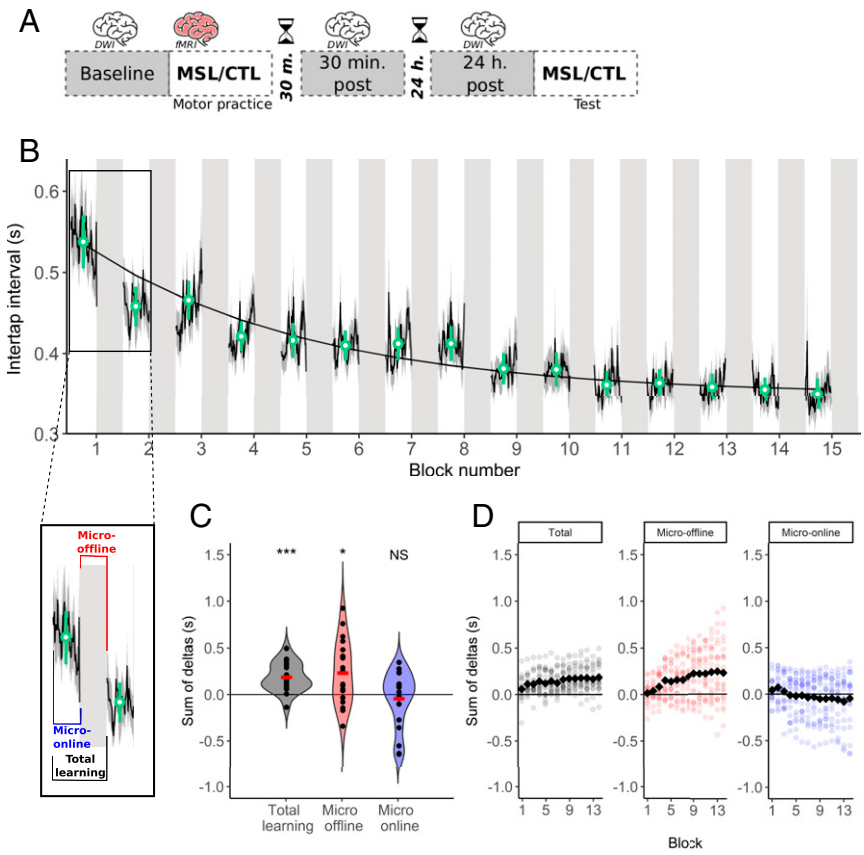

Fig. 1. Experimental design and behavior. (*A*) Experimental design. Twenty participants trained on two sensorimotor tasks: MSL (7) and an active CTL. Functional images (fMRI) were obtained during training on the MSL task. DWIs were acquired for both tasks before and 30 min and 24 h after practice. Long-term memory was assessed at *Test*, 24 h after practice. (*B*) Motor sequence learning. During motor practice, MSL was quantified using the intertap interval (depicted in black), i.e., the time elapsed between successive key presses from correctly executed sequences. Green dots represent the mean intertap interval ± SE for each block. Rest periods between task blocks are indicated with vertical gray bars. *Inset* illustrates the different learning metrics quantified for each block: MOnGs, MOGs, and total learning. MOGs were calculated as the difference (delta) in the mean intertap interval between the last correct sequence of a block and the first correct sequence of the next block, whereas MOnGs were quantified as the difference between the first and last correct sequence within a block. Total learning reflects the sum of MOnGs and MOGs. (*C*) MOGs and MOnGs. Data points in the violin plots depict the sum of deltas for each learning metric over all blocks across participants (***$P < 0.0001$; *$P < 0.05$, NS: not significant, *t* test against zero, corrected by Bonferroni). A linear regression analysis indicated that total learning was explained by MOGs (MOGs: $F(1,18) = 4.5371$, $P = 0.047$; MOnGs:$F(1,18) = 7e\text{-}04$, $P = 0.98$). Furthermore, MOGs differed from MOnGs (paired *t* test, $t_{19} = 1.99$, $P = 0.03$). (*D*) Cumulative sum of changes in performance as a function of block number. This measure was computed based on the cumulative sum of deltas for all blocks. Note that MOGs take place during the first half of learning, before reaching asymptotic performance.

role of the hippocampus in short-term memory stabilization that may differ from its role in sleep-dependent consolidation (12).

Interestingly, both the left hippocampus and the right precuneus exhibited learning-induced changes in microstructure 30 min after practice, reflected as a reduction in MD (Fig. 2*B*) (motor regions did not survive family-wise error correction). Remarkably, the decrease in MD observed in the precuneus persisted 24 h later. The extent of the anatomical overlap between our functional and structural results is better appreciated in Fig. 2*C*. A marginally significant relationship between the decrease in hippocampal MD observed at 30 min and its functional activity during rest ($r = 0.42$, $P = 0.065$) suggests that subjects exhibiting stronger hippocampal activity during rest periods tended to undergo greater structural changes. Altogether, the functional and structural findings presented above suggest that the same network that reactivates during the quiet rest periods of training undergoes structural plasticity, a mechanism in line with the modern definition of an engram (9).

How may the hippocampus contribute to motor learning? In a unifying view, Buzsáki and Tingley proposed that the hippocampus may act as a sequence generator, connecting encoded items of different modalities in space/time through specific cortical connections via sharp-wave ripples (13). We speculate that during MSL the hippocampus may reactivate information about the sequence leading to MOGs. This phenomenon, like memory replay described in rodents, is more evident during quiet rests (6) and more prominent during early stages of learning (14). The strong functional connectivity observed here between the hippocampus and the limbic portion of the precuneus, one of the main outputs relaying information to the neocortex (15), suggests that plastic changes detected with DWI 30 min postpractice emerge from their close interaction during learning and thereafter.

Our work advances the field of learning and memory at multiple levels. First, it shows that the hippocampus is associated with the generation of MOGs through a mechanism reminiscent of memory reactivation (14). Second, it provides compelling evidence suggesting that this potential reactivation impacts on the microstructure of the hippocampus. Third, it suggests that motor memories may originate from an early interplay between the hippocampus and the cortex. This is in line with recent studies on declarative memory (8, 9) challenging the dominant

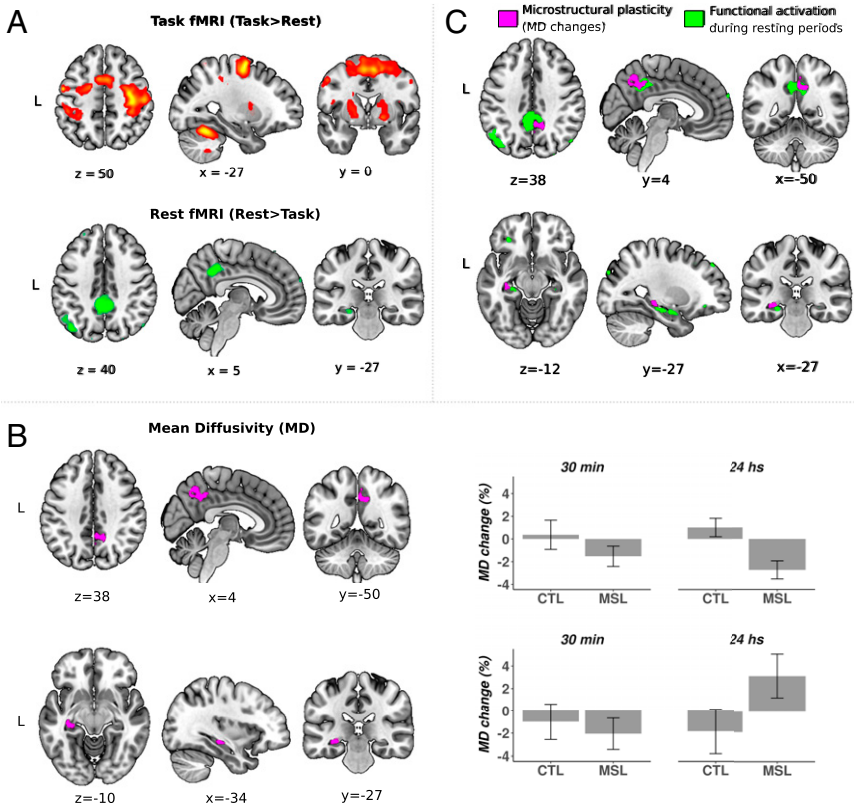

Fig. 2. Tracking functional and microstructural changes induced by MSL. (*A*) Functional changes observed during motor learning. Shown are the whole-brain, voxelwise statistical parametric maps (SPMs) for the Task (Task > Rest) and Rest (Rest > Task) periods ($P < 0.05$, FWE-corrected). Note that cortico-cerebellar and cortico-striatal systems were activated during task execution (in red), whereas the hippocampus and the precuneus increased their activity during the rest periods (in green). (*B*) Longitudinal changes in microstructure induced by MSL. To identify longitudinal changes in microstructure that differed across scanning sessions and tasks, we conducted a whole-brain, voxelwise task (MSL vs. CTL) by scanning session (baseline, 30 min, 24 h) interaction analysis (FWE-corrected *P* value <0.05). Barplots show the mean and the 95% CIs corresponding to the time course of MD for each cluster identified in this analysis. Note that MSL induced changes in MD in the hippocampus and the precuneus. (*C*) Overlap between functional and structural changes induced by MSL. Shown are the SPMs resulting from the Rest fMRI analysis (in green) overlaid on the MD analysis (in magenta).

view of systems consolidation as a slow transfer from the hippocampus to the neocortex. Our findings support recent work pointing to the involvement of the hippocampus in the reactivation of procedural memories (7, 12, 16, 17) and provide evidence for a possible common mechanism at the basis of the formation of declarative and nondeclarative memories (13).

Materials and Methods

Participants. Twenty subjects between 18 and 31 y old (10 female; ages: mean ± SD = 23.6 ± 3.1) participated in the study. All participants were healthy volunteers with no self-reported history of psychiatric, neurological, or cognitive impairment, nor any history of sleep disturbances. None of them had previous experience playing a musical instrument. Also, none of the subjects worked night shifts or were engaged in transmeridian trips 6 mo before the study. Subjects were asked to abstain from alcohol and caffeine the day before and during the experiment. They were also instructed to maintain their regular sleep habits.

All subjects were right-handed as assessed by the Edinburgh handedness inventory (18). Participants provided written consent and were paid for their participation. The experimental procedure was approved by the local Ethics Committee (University of Buenos Aires) and performed according to the Declaration of Helsinki.

Experimental Design and Paradigms. Twenty participants trained on three sensorimotor tasks separated by 1 wk: an MSL task, a visuomotor adaptation task, and an active control (CTL) task involving no learning. The order of practice on these tasks was counterbalanced. Only the data corresponding to the MSL and CTL tasks is reported here.

DWI, T1-weighted (T1w), and BOLD fMRI images were acquired during this study. DWIs were obtained before practice (baseline) and 30 min and 24 h postpractice to assess changes in microstructure. BOLD images were obtained during MSL training only (Fig. 1*A*).

Motor tasks. The MSL task required subjects to press a series of four keys with the fingers of the nondominant hand following a sequence of movements of five elements (4-1-3-2-4, 4 being the index finger and 1 being the pinky finger) (7, 19). The objective of the task was to execute the sequence as quickly and accurately as possible. In the motor practice session, which lasted around 15 min, subjects executed the motor sequence in a self-paced manner in 15 blocks of 60 key presses separated by rest periods of 25 s. A test session, which comprised another 8 blocks of practice of the same task, was also carried out 24 h postpractice to assess long-term memory retention and took place after MRI acquisition.

The CTL task accounted for the sensorimotor aspects of the MSL task. Subjects had to press a button in response to a green target appearing on a screen ($P = 0.9$) and withhold from responding whenever the target was red ($P = 0.1$). The duration of the motor practice session for the CTL condition lasted approximately the same as the MSL task.

Experimental paradigms were programmed using MATLAB's Psychophysics Toolbox, Version 3 (20).

Motor sequence learning quantification. Motor sequence learning was quantified using the intertap interval, i.e., the time elapsed between successive key presses from correctly executed sequences. The mean intertap interval was calculated for each block and for all subjects. For illustration purposes, the intertap intervals from correct sequences in each block were averaged for all subjects, and a five-element moving average filter (current element, 2 forward, and 2 backward) was applied to smooth the data.

Micro-online gains (MOnGs) were calculated as the difference (delta) in mean intertap interval of the first and last correct sequence within a block of practice, while MOGs were computed as the difference between the mean intertap interval of the last correct sequence of a practice block and the first correct sequence of the following block. Finally, the total learning per block was calculated as the difference between the mean intertap interval of the first correct sequence within a practice block compared to the mean intertap interval of the first sequence of the following practice block. Hence, the total learning within a practice block consisted of the sum of the MOnGs and MOGs. The amount of MOGs, MOnGs, and total learning was quantified as the sum of deltas within each block for all blocks. Learning for each of these metrics was assessed by running a *t* test against zero (*P* values were corrected for the multiple comparisons using Bonferroni). To examine whether total learning could be better explained by MOGs or MOnGs, we conducted a regression analysis. To this aim, we used the function *lm* from the *stats* package in R (21) to fit a linear model with total learning as response variable and either MOGs or MOnGs as explanatory variables. In addition, we conducted a paired *t* test to confirm this effect by directly comparing MOGs and MOnGs. Finally, to assess how these quantities evolved over blocks, we computed the cumulative sum of deltas as a function of block number.

Differences in MOGs as a function of learning were assessed by dividing the practice session in two stages of learning: early (blocks 1–7) and late (blocks 8–14). Note that MOGs could not be computed for the 15th block, as it was the last one. For each subject, we calculated the median MOGs across both stages of learning. Prior to statistical testing, outliers were detected based on a threshold of two median absolute deviations (MAD) from the group median and removed from the corresponding analyses (22). We assessed behavioral differences between learning stages by fitting a linear mixed model in R (21) using the function *gls* from the *nlme* package, with learning stage (Early; Late) as the fixed effect, and Subject as the random effect. The variance was modeled for each stage separately to account for heteroskedasticity [Levene's test, $F(1,30) = 11.86$, $P = 0.002$].

In order to assess whether MOGs impacted on overnight offline gains, for each subject we computed the percent difference in performance at the end of the motor practice session vs. the beginning of the Test session (overnight offline gains). Specifically, it was calculated as the difference between the average intertap interval of the last three blocks of the motor practice session and the first three blocks of the Test session relative to the former. A Pearson correlation was conducted in R (21) to assess the degree of association between the sum of MOGs for all blocks and the overnight offline gains.

The significance threshold was set at $P < 0.05$ for all statistical tests, unless otherwise specified. Due to loss of the behavioral data, one subject had to be excluded from MSL quantification and MOG-related analyses.

Acquisition and Processing of Magnetic Resonance Images. Magnetic resonance images (MRI) were acquired with a 3T Siemens Tim TRIO scanner using a 12-channel head RF receive coil (Instituto Angel Roffo, University of Buenos Aires).

T1w images. T1w volumes used for normalization of DWI and BOLD images were acquired using the MP2RAGE WIP sequence (23), with the following parameters: repetition time (TR) = 5,000 ms; echo time (TE) = 2.89 ms; flip angle (FA) 1 = 4°; FA2 = 5°; Inversion Time (TI) 1 = 700 ms; TI2 = 2,500 ms; bandwidth (BW) = 240 Hz/Px; field-of-view (FOV)= 256 × 256 mm^2; acquisition matrix = 256 × 256; voxel size = 1 × 1 × 1 mm^3; slices = 176; parallel acquisition = GRAPPA mode, acceleration factor 2. The acquisition was performed in sagittal slices along the *y-z* plane of the static magnetic field reference frame. The T1-uniden (T1w denoised) image was used for the coregistration and subsequent normalization of functional images.

fMRIs.

Acquisition and preprocessing. fMRIs were acquired during MSL using the multiband-accelerated sequence implemented by the Center for Magnetic Resonance Research (24, 25). The following protocol was used for acquisition: voxel size = 3 × 3 × 3 mm^3, FOV = 192 × 192 mm, 42 slices aligned with the AC-PC line, 10% gap, posterior-anterior (P-A) phase encoding direction, TR = 1,433 ms, TE = 30 ms, multiband acceleration factor = 2, no PAT, BW = 1,502 Hz/Px, echo spacing = 0.75 ms, EPI factor = 64, FA = 69°.

A gradient echo field map was also acquired for posterior correction of field inhomogeneities. The following acquisition parameters were used: 42 slices, 20% gap, voxel size = 3 × 3 × 3 mm^3, FOV = 192 × 192 mm, P-A phase-encoding direction, TR = 444 ms, TE1 = 4.92 ms, TE2 = 7.38 ms, FA = 44°, BW = 260 Hz/px.

The dicom images were converted to nifty format using the dcm2nii software (26). Preprocessing and analysis were performed using the Statistical Parametric Mapping software SPM12 (Wellcome Department of Cognitive Neurology). The functional time series was motion corrected, using the middle volume of the series as reference. Since the experimental paradigm consisted of a block design, we did not perform slice-timing correction. Correction of magnetic field inhomogeneities was then performed using the gradient-echo field map. The same process was applied to the Single-Band Reference (SBRef) image, a single-volume, high-contrast EPI image acquired in the same space as the fMRI data (27). The resulting realigned and unwarped images were then merged and coregistered to the corresponding high-resolution T1w image for each subject via the SBRef image. A nonlinear registration was carried out from the T1w in subject space to the 2-mm T1w MNI template. Finally, transformations were concatenated and the resulting images were resliced and smoothed with a Gaussian kernel of 8-mm full-width at half-maximum.

Data analysis and statistics. We performed a standard whole-brain voxelwise general linear model (GLM) analysis to assess the brain regions active during motor execution (Task > Rest) and during the rest periods (Rest > Task) using SPM12 (WellcomeTrust Center for Neuroimaging, University College London). Then we asked whether the parameter estimates (beta weights) of this GLM were significantly different from zero using a one-tailed *t* test for each condition. Active areas during each condition were defined using a $P < 0.05$ threshold, corrected for family-wise errors (FWE) using random-field theory.

Differences in the BOLD signal across learning were assessed by dividing the practice session in two stages: early (blocks 1–7) and late (blocks 8–14). To keep coherence with the behavioral (MOGs) analysis, we excluded the 15th block from this analysis too. For each subject, the mean BOLD signal within each cluster identified in the Rest > Task contrast (precuneus and hippocampus) was extracted using the MarsBar tool for SPM (http://marsbar.sourceforge.net/). Then, using custom scripts, the data points for each condition (Rest and Task) were averaged within each block. For each subject, we calculated the median BOLD signal difference (Rest-Task) across learning stages.

Prior to statistical testing, outliers were detected based on a threshold of two MADs from the group median and removed from the corresponding analyses (22). We assessed differences between both learning stages by fitting a linear mixed model in R (21) using the function *lme* from the *nlme* package, with learning stage (Early; Late) as fixed effect and Subject as random effect. The resulting *P* values were corrected for multiple tests (one test per cluster) using Bonferroni.

We ran a Pearson correlation in R (21) to assess the degree of association between the median difference in BOLD signal between conditions (Rest-Task) extracted for each cluster and the median MOGs on each learning stage.

To assess the degree of connectivity between the hippocampus and the precuneus throughout motor sequence learning, we ran a repeated-measures correlation of the BOLD signal for both clusters for all blocks of the Rest and Task conditions. For this purpose, we used the *rmcorr* package in R (21). Briefly, the repeated-measures correlation is a statistical technique for determining the common within-individual association for paired measures assessed on two or more occasions for multiple individuals (28).

DWIs.

Acquisition and preprocessing. DWIs were acquired using the multiband-accelerated sequence implemented by the Center for Magnetic Resonance Research (24, 25). The following protocol was used for acquisition: voxel size = 2 × 2 × 2 mm^3; FOV = 240 × 240 mm^2; 30 monopolar gradient directions uniformly distributed (29, 30); 70 axial slices; TR = 5,208 ms; TE = 89 ms; acquisition time (TA) = 3 min and 34 s; BW = 1,488 Hz/Px; multiband acceleration factor = 2, SENSE1 coil-combine mode, pure axial slice orientation with interleaved slice acquisition, anterior-posterior (A-P) phase encoding direction, with a b value = 1,000 s/mm^2. Phase encoding in A-P direction was chosen to preserve hemispheric symmetry (31). Eight b0 volumes were acquired using an A-P phase encoding direction: two were acquired at the beginning of the sequence, one at the end, and the rest interleaved every five b-1000 volumes. This configuration optimizes the signal-to-noise ratio of scalar images resulting from the fit of a diffusion tensor model (30). In addition, one b0 volume was acquired with P-A phase encoding direction to correct for susceptibility-induced geometric distortions (32).

DWI dicom images were converted to nifty format using the dcm2nii software (26). Preprocessing steps for DWI were conducted for each of the scanning sessions separately, and included 1) correction of susceptibility-induced distortions using FSL's topup tool with b0 volumes acquired with opposite phase encoding direction (32) and 2) correction of eddy currents-induced distortions, head motion correction, and b-vector rotation using

FSL's eddy tool (33) (version 5.0.9). Next, DTIfit (FSL) was used to fit a diffusion tensor model to produce the scalar measures of interest: fractional anisotropy (FA) and MD. After preprocessing, the diffusion tensor imaging (DTI) scalar maps were normalized to MNI152 stereotaxic space using an ANTs-based pipeline created by our group that minimizes across-session test-retest reproducibility error (34). Briefly, this pipeline uses ANTs to nonlinearly register FA images to the MNI152 T1 template via a subject-specific intermediate FA template constructed from the FA images from each subject's sessions. Normalized DTI measures were smoothed using a 4-mm full-width at half maximum (FWHM) Gaussian kernel.

Data analysis and statistics. Whole-brain voxelwise longitudinal MD changes associated with motor learning were statistically assessed using the Sandwich Estimator (SwE) toolbox for accurate modeling of longitudinal and repeated-measures neuroimaging data (35). We used a nonparametric threshold-free cluster enhancement inference approach (36) with 1,000 permutations and a FWE-corrected P value <0.05. In order to identify changes in microstructure that differed across scanning sessions and tasks, we ran a task (MSL vs. CTL) by scanning session (baseline, 30 min, and 24 h) interaction analysis.

To examine the time course of MD, we extracted all of the voxels for each cluster and each subject identified from the task-by-scanning session interaction using FSL's fslmeants tool with the "showall" option. Then, we calculated the median MD within each cluster using custom scripts in R (21) for each subject, task, and session. Percent MD changes at 30 min and 24 h were then calculated for each subject and task by subtracting and dividing by the baseline MD value. Prior to the assessment of descriptive statistics, outliers were detected based on a threshold of two SDs from the group average and were removed from the corresponding analyses. For each task and time-point, we calculated the mean across subjects and 95% CIs of the percent MD changes using the *summarySEwithin* function from the *Rmisc* package from R (21). This function normalizes within-subject data to remove the between-subject variability and computes the variance from this normalized data using the method from Morey (37).

Finally, to explore the connection between functional changes in the hippocampus related to MOGs and neuroplasticity, the mean beta weight from the second level GLM analysis for the voxels within the hippocampus cluster was extracted using the fslmeants function from FSL. Next, we ran a Pearson correlation in R (21) to assess the degree of association between the beta weight and the MD decrease at 30 min.

Limitations interpreting changes in mean diffusivity. DTI is a mathematical model for diffusion MRI data that allows estimation of metrics sensitive to tissue microstructure, such as MD. The diffusion of water in brain tissue may be affected by a combination of effects, including local cell geometry, viscosity, and tissue membrane permeability (38–40). The estimates of MD therefore reflect the average hindrance of water diffusion in the voxel. However, given the limited duration of human experiments, it is difficult to identify the specific factors that may drive the hindrance at the cellular level (41, 42). This represents a limitation for interpreting MD changes, which reflect a combination of intracellular and extracellular water diffusion effects. To address such limitations, recent DTI and histological studies have evaluated associations between in vivo and ex vivo cellular effects. Specifically, Assaf and coworkers (8, 43) have shown that plasticity induced in the hippocampus of rats during learning in the Morris water maze is associated with an increase in synaptogenesis and astrocyte perimeter (glial hypertrophy), and that this increase in tissue density is accompanied by a reduction in MD.

It is important to emphasize, however, that given that MD is not specific to intracellular or extracellular compartments, a further growth of the intracellular compartment due to a progressive increment in astrocyte perimeter and neuronal surface may potentially lead to an increase in MD with the passage of time. In other words, the intracellular compartment may become more salient than the extracellular compartment leading to a switch in MD from an initial net reduction to a later increment.

Data Availability. The dataset and scripts used to process and analyze the data can be accessed upon request from Zenodo (https://doi.org/10.5281/zenodo.3996736).

ACKNOWLEDGMENTS. This work was supported by a collaborative grant from the Quebec Bioimaging Network (Canada), a grant from the Argentinian Ministry of Defense, and National Agency for the Promotion of Science and Technology Grant PICT-2015-0488.

1. A. S. Gupta, M. A. A. van der Meer, D. S. Touretzky, A. D. Redish, Hippocampal replay is not a simple function of experience. *Neuron* **65**, 695–705 (2010).
2. A. Tambini, L. Davachi, Persistence of hippocampal multivoxel patterns into post-encoding rest is related to memory. *Proc. Natl. Acad. Sci. U.S.A.* **110**, 19591–19596 (2013).
3. A. Tambini, N. Ketz, L. Davachi, Enhanced brain correlations during rest are related to memory for recent experiences. *Neuron* **65**, 280–290 (2010).
4. A. C. Schapiro, E. A. McDevitt, T. T. Rogers, S. C. Mednick, K. A. Norman, Human hippocampal replay during rest prioritizes weakly learned information and predicts memory performance. *Nat. Commun.* **9**, 3920 (2018).
5. M. Bönstrup *et al*., A rapid form of offline consolidation in skill learning. *Curr. Biol.* **29**, 1346–1351.e4 (2019).
6. B. E. Pfeiffer, D. J. Foster, Hippocampal place-cell sequences depict future paths to remembered goals. *Nature* **497**, 74–79 (2013).
7. G. Albouy *et al*., Maintaining vs. enhancing motor sequence memories: Respective roles of striatal and hippocampal systems. *Neuroimage* **108**, 423–434 (2015).
8. Y. Sagi *et al*., Learning in the fast lane: New insights into neuroplasticity. *Neuron* **73**, 1195–1203 (2012).
9. S. Brodt *et al*., Fast track to the neocortex: A memory engram in the posterior parietal cortex. *Science* **362**, 1045–1048 (2018).
10. I. Tavor, R. Botvinik-Nezer, M. Bernstein-Eliav, G. Tsarfaty, Y. Assaf, Short-term plasticity following motor sequence learning revealed by diffusion magnetic resonance imaging. *Hum. Brain Mapp.* **41**, 442–452 (2019).
11. J. Doyon, V. Penhune, L. G. Ungerleider, Distinct contribution of the cortico-striatal and cortico-cerebellar systems to motor skill learning. *Neuropsychologia* **41**, 252–262 (2003).
12. A. C. Schapiro *et al*., The hippocampus is necessary for the consolidation of a task that does not require the hippocampus for initial learning. *Hippocampus* **29**, 1091–1100 (2019).
13. G. Buzsáki, D. Tingley, Space and time: The Hippocampus as a sequence generator. *Trends Cognit. Sci.* **22**, 853–869 (2018).
14. D. J. Foster, Replay comes of age. *Annu. Rev. Neurosci.* **40**, 581–602 (2017).
15. D. S. Margulies *et al*., Precuneus shares intrinsic functional architecture in humans and monkeys. *Proc. Natl. Acad. Sci. U.S.A.* **106**, 20069–20074 (2009).
16. A. Sawangjit *et al*., The hippocampus is crucial for forming non-hippocampal long-term memory during sleep. *Nature* **564**, 109–113 (2018).
17. J. Döhring *et al*., Motor skill learning and offline-changes in TGA patients with acute hippocampal CA1 lesions. *Cortex* **89**, 156–168 (2017).
18. R. C. Oldfield, The assessment and analysis of handedness: The Edinburgh inventory. *Neuropsychologia* **9**, 97–113 (1971).
19. K. Debas *et al*., Brain plasticity related to the consolidation of motor sequence learning and motor adaptation. *Proc. Natl. Acad. Sci. U.S.A.* **107**, 17839–17844 (2010).
20. D. H. Brainard, The Psychophysics toolbox. *Spat. Vis.* **10**, 433–436 (1997).
21. R Core Team, *R: A Language and Environment for Statistical Computing*, (R Foundation for Statistical Computing, Vienna, Austria, 2017).
22. C. Leys, C. Ley, O. Klein, P. Bernard, L. Licata, Detecting outliers: Do not use standard deviation around the mean, use absolute deviation around the median. *J. Exp. Soc. Psychol.* **49**, 764–766 (2013).
23. J. P. Marques *et al*., MP2RAGE, a self bias-field corrected sequence for improved segmentation and T1-mapping at high field. *Neuroimage* **49**, 1271–1281 (2010).
24. K. Uğurbil *et al*.; WU-Minn HCP Consortium, Pushing spatial and temporal resolution for functional and diffusion MRI in the Human Connectome Project. *Neuroimage* **80**, 80–104 (2013).
25. J. Xu *et al*., Evaluation of slice accelerations using multiband echo planar imaging at 3 T. *Neuroimage* **83**, 991–1001 (2013).
26. X. Li, P. S. Morgan, J. Ashburner, J. Smith, C. Rorden, The first step for neuroimaging data analysis: DICOM to NIfTI conversion. *J. Neurosci. Methods* **264**, 47–56 (2016).
27. M. F. Glasser *et al*.; WU-Minn HCP Consortium, The minimal preprocessing pipelines for the Human Connectome Project. *Neuroimage* **80**, 105–124 (2013).
28. J. Z. Bakdash, L. R. Marusich, Repeated measures correlation. *Front. Psychol.* **8**, 456 (2017).
29. D. K. Jones, The effect of gradient sampling schemes on measures derived from diffusion tensor MRI: A Monte Carlo study. *Magn. Reson. Med.* **51**, 807–815 (2004).
30. D. K. Jones, M. A. Horsfield, A. Simmons, Optimal strategies for measuring diffusion in anisotropic systems by magnetic resonance imaging. *Magn. Reson. Med.* **42**, 515–525 (1999).
31. S. M. Smith *et al*., Acquisition and voxelwise analysis of multi-subject diffusion data with tract-based spatial statistics. *Nat. Protoc.* **2**, 499–503 (2007).
32. J. L. R. Andersson, S. Skare, J. Ashburner, How to correct susceptibility distortions in spin-echo echo-planar images: Application to diffusion tensor imaging. *Neuroimage* **20**, 870–888 (2003).

33. J. L. R. Andersson, S. N. Sotiropoulos, An integrated approach to correction for off-resonance effects and subject movement in diffusion MR imaging. *Neuroimage* **125**, 1063–1078 (2016).
34. F. Jacobacci *et al*., Improving spatial normalization of brain diffusion MRI to measure longitudinal changes of tissue microstructure in the cortex and white matter. *J. Magn. Reson. Imaging*, 10.1101/590521 (2020).
35. B. Guillaume, X. Hua, P. M. Thompson, L. Waldorp, T. E. Nichols; Alzheimer's Disease Neuroimaging Initiative, Fast and accurate modelling of longitudinal and repeated measures neuroimaging data. *Neuroimage* **94**, 287–302 (2014).
36. S. M. Smith, T. E. Nichols, Threshold-free cluster enhancement: Addressing problems of smoothing, threshold dependence and localisation in cluster inference. *Neuroimage* **44**, 83–98 (2009).
37. R. D. Morey, Confidence intervals from normalized data: A correction to Cousineau (2005). *Tutor. Quant. Methods Psychol.* **4**, 61–64 (2008).
38. P. J. Basser, Inferring microstructural features and the physiological state of tissues from diffusion-weighted images. *NMR Biomed.* **8**, 333–344 (1995).
39. P. J. Basser, C. Pierpaoli, Microstructural and physiological features of tissues elucidated by quantitative-diffusion-tensor MRI. *J. Magn. Reson. B.* **111**, 209–219 (1996).
40. C. Beaulieu, The basis of anisotropic water diffusion in the nervous system–A technical review. *NMR Biomed.* **15**, 435–455 (2002).
41. Y. Assaf, R. Z. Freidlin, G. K. Rohde, P. J. Basser, New modeling and experimental framework to characterize hindered and restricted water diffusion in brain white matter. *Magn. Reson. Med.* **52**, 965–978 (2004).
42. D. K. Jones, T. R. Knösche, R. Turner, White matter integrity, fiber count, and other fallacies: The do's and don'ts of diffusion MRI. *Neuroimage* **73**, 239–254 (2013).
43. I. Tavor, S. Hofstetter, Y. Assaf, Micro-structural assessment of short term plasticity dynamics. *Neuroimage* **81**, 1–7 (2013).